Electrochimica Acta 136 (2014) 404–411

Contents lists available at ScienceDirect

Electrochimica Acta

journal homepage: www.elsevier.com/locate/electacta

Preparation and Characterization of TiO_2 Nanotube Arrays in Ionic Liquid for Water Splitting

R.G. Freitas, M.A. Santanna, E.C. Pereira*

NANOFAEL – LIEC – Departamento de Química. Universidade Federal de São Carlos – C.P.: 676 – CEP: 13565-905, São Carlos, SP, Brazil

ARTICLE INFO

Article history:
Received 27 March 2014
Accepted 18 May 2014
Available online 27 May 2014

Keywords:
TiO_2 nanotubes
water splitting
electron lifetime
photocurrent transients

ABSTRACT

In the present work, it is described the fabrication and characterization of TiO_2 nantotubes prepared potentiostatically using 1.0 or 5.0 vol.% ionic liquid electrolyte medium at 10 or 20 °C. These experimental conditions led to TiO_2 nanotubes with 63-77 nm pore diameter, crystallite sizes between 27-33 nm, and band-gap values in the 3.1-3.2 eV range. Although the morphology and band-gap values were similar, the water splitting reaction showed differences in terms of photocurrent, up to 300%. Besides, we report also important changes in those parameters related with electronic defects, such as carrier density (N_D), width of depletion layer (w) and Debye length (λ_D). Then, the enhancement on photoelectrochemical properties could be related to a decrease in the rate of surface recombination processes. Finally, these proposition are in agreement with the open-circuit voltage-decay, where was observed a higher electron lifetime for TiO_2NT obtained at higher vol.% of ionic liquid.

1. Introduction

Efficient splitting of water into H_2/O_2, photocatalytically activated, is probably the most desired pathway to convert abundant solar energy into "hydrogen", the proposed clean energy carrier of the future. The total amount of solar energy impinging on the earth's surface in one year is about $3x10^{24}$ J, or approximately 10^4 times the worldwide yearly consumption of energy [1]. The search for efficient conversion of solar energy into other useful forms is, in view of the increasing anxiety over the exhaustion of fossil energy resources and attendant global warming, one of the most important challenges for future.

However, there are three major important tasks for the solar production of hydrogen: *(1) Stability*. Metal oxides are the most photochemically stable semiconductors in aqueous solution, but their band-gaps are either too large (≈3.0 eV) to absorb a significant fraction of incident solar energy, or their semiconductor characteristics (e.g. charge transport) are poor [2]. *(2) Band-gap values*. Considering the water splitting energy of 1.23 eV and overpotential losses, the semiconductor(s) should have a band-gap greater than 1.7 eV. However, semiconductors with relative low band-gaps have been found to lack stability during water splitting [2]. *(3) Energy level edge position*. Even though a semiconductor may generate sufficient energy to drive an electrochemical reaction, the band edge position may prevent it from react leading to water splitting [2]. For spontaneous water splitting, water oxidation and reduction potential must lie between the valence and conduction band edges.

Among inorganic oxides, TiO_2 is an important candidate for efficiently water splitting reaction. Several papers in the literature [3,4] have demonstrated that besides the microstructure, the morphology is important to optimize the oxide properties. Then, TiO_2 nanotubes (TiO_2NT) seem to be a promise material as photoanode to water splitting application, once these nanostructures provide unique electronic properties, such as high electron mobility [5], appropriated band edge positions [6], quantum confinement effects [7], high specific surface area [8], high mechanical strength [9] and photocorrosion resistance [10]. In this scenario, TiO_2NTs seem to be a versatile compound and one of the most investigated nanostructure in materials science.

Among the factors that affect the TiO_2NT properties, electrochemically obtained, the non-aqueous electrolyte can be regarded as a very important variable. In this context, ionic liquid (IL) have many applications, such as powerful solvents and electrically conducting fluids (electrolytes). Specifically during titanium anodization, the use of a fluor salt which is liquid at ambient temperature, such as 1-butyl-3-methyl-imidazolium-tetrafluoroborate (BMIM-BF_4), is important as fluoride precursors source which determine the quality, morphology and density of the nanotubes. The use of ionic liquid as electrolyte during the TiO_2NTs obtainment by electrochemical means is quite recent, and just few papers have reported it. Schmuki et al. [11] observed the formation of well-ordered self-organized TiO_2 nanotube layers in BMIN-BF_4

* Corresponding author. Tel.: +55 16 3351 8214; fax: +55 16 3351 8214.
E-mail addresses: ernesto@ufscar.br, ernestopereira51@gmail.com (E.C. Pereira).

http://dx.doi.org/10.1016/j.electacta.2014.05.097
0013-4686/

Table 1
Experimental conditions in which TiO_2NT arrays were obtained.

TiO_2NT	Vol.% IL	T/°C
1	1.0	10
2	5.0	10
3	1.0	20
4	5.0	20

ionic liquid electrolyte. According to the authors, by changing the potential and anodization time, the maximum thickness achieved was approximately 650 nm and the maximum diameter obtained was around 43 nm. Misra et al. [12] for the first time in the literature, synthesized double-wall vertically oriented TiO_2NT arrays by a simple sonoelectrochemical anodization process using BMIM-BF_4 ionic liquid at room-temperature. The concentric nanotubes with external diameters of around 82 and 206 nm were obtained by this process. In addition to the double-wall nature of these nanotubes, the external diameter of >200 nm is the largest among all the anodization processes. Teixeira et al. [13] observed that a maximum nanotube growth rate was obtained at 1.0 vol % BMIM-BF_4. Furthermore, the TiO_2 nanotubes obtained showed photocatalytic activities for the degradation of pollutants using methyl orange dye as a prototype and hydrogen generation by water splitting.

In light of this, the present study aims to investigate how structural (crystallite size) and electronic parameters (flatband potential, carrier density, width depletion layer, Debye screening length) affect the photoelectrocatalysis towards the water splitting reaction.

2. Experimental

2.1. Preparation of the TiO_2 nanotube arrays

Self-ordered TiO_2NT arrays were prepared by anodizing 1 cm^2 of titanium foil (99.8% Alfa Aesar) in electrolytes composed of ethylene glycol (Synth), Milli-Q water (10 vol. %) and 1-butyl-3-methyl-imidazolium-tetrafluoroborate (BMIM-BF_4 Sigma Aldrich) (1 or 5 vol. %). Prior to each anodization, Ti samples were ultrasonicated in acetone followed by distilled water rinses and dried in N_2 stream. Anodization was performed at 10 and 20 °C using a standard two-electrode cell with Ti foil as anode and a platinum foil (4 cm^2) as cathode, which underwent a constant applied voltage of 80 V, using a Keithley 2410 sourcemeter. The voltage was swept from the OCP to different values at $\nu = 0.1$ V s^{-1}, holding at the final potential value for 4 hours. The TiO_2NT photoelectrodes herein prepared and discussed along the text are specified in Table 1. After the anodization process, the samples were rinsed with distilled water and thermally treated at 450 °C for 120 minutes to eliminate water, organic portions, improve its mechanical stability and to obtain the TiO_2-anatase crystalline phase. Soon after, a cooling rate of 5 °C min^{-1} was used.

2.2. Material Characterization

The TiO_2NTs morphological characterization was carried out using a Supra 35 Zeiss Field Emission Scanning Electron Microscope. The optical absorption spectra were obtained using a UV-vis spectrometer (UV-vis DRS; Cary 5G). The X-ray diffraction (XRD) patterns were obtained using a Siemens diffractometer model D-5000 with CuKα radiation and λ = 1.5406 Å.

2.3. Photoelectrochemical Activity and Water Splitting Generation

Photoelectrochemical measurements were performed in the photocell with a quartz ($d = 3$ cm) window. The photoelectrochemical measurements were performed using an Autolab PGSTAT-30 Potentiostat/Galvanostat. Platinum wire and TiO_2NTs were respectively used as counter and working electrodes. All potential were referred to the reversible hydrogen electrode (RHE). Photoelectrochemical test were carried out using 0.5 M H_2SO_4 solution as electrolyte. A solar simulator (Newport Oriel Arc lamp housing 67005, Oriel xenon lamp 6255, Oriel arc lamp power supply 69907 USA) was used as light source.

3. Results and discussion

Current-time curves obtained during the formation of the TiO_2 nanotube arrays films in BMIM-BF_4 ionic liquid at 80 V are shown in Fig. 1.

Similar current-time profile was observed for all TiO_2NT electrodes. A sharp drop in current was observed in the first stage due to the formation of a barrier oxide layer; followed by an increase in current caused by the oxide layer pitting by fluoride ions and finally, the current reaches a steady value This behaviour follows in agreement with the literature [14]. Electrodes TiO_2NT-1 and 2 exhibited lower current values compared to TiO_2NT-3 and 4, what can be related to the lower temperature (10 °C) used during the anodization process. Additionally, it is possible to observe that the current values increase for higher ionic liquid concentrations, e.g. 1 and 5%, as can be observed for TiO_2NT-1, 3 (1 vol.% IL) and TiO_2NT-2, 4 (5 vol. % IL). Again, it agrees with the reported characteristics of Ti in F^- containing electrolyte described by in the literature [15].

The surface morphology of TiO_2NT was investigated by FESEM microscopy and is depicted in Fig. 2.

The average pore diameter obtained at 10 °C was around 77.5 ± 2.4 nm and 64.0 ± 2.5 nm for samples obtained in 1vol.% and 5vol.% of IL respectively. For nanotubes obtained at 20 °C, the pore diameter were approximately 75.8 ± 2.8 nm and 68.0 ± 2.0 nm for samples obtained in 1vol.% and 5vol.% IL respectively. It is possible to observe that TiO_2NTs prepared at higher percentages of IL lead to a decreasing in the tube diameter comparing the samples prepared at the same anodization temperature. Although the TiO_2NT photoelectrodes do not show any significant difference from a morphologic point of view, the synthesis conditions resulted in significant differences regarding the structural and electronic properties, as will be discussed below.

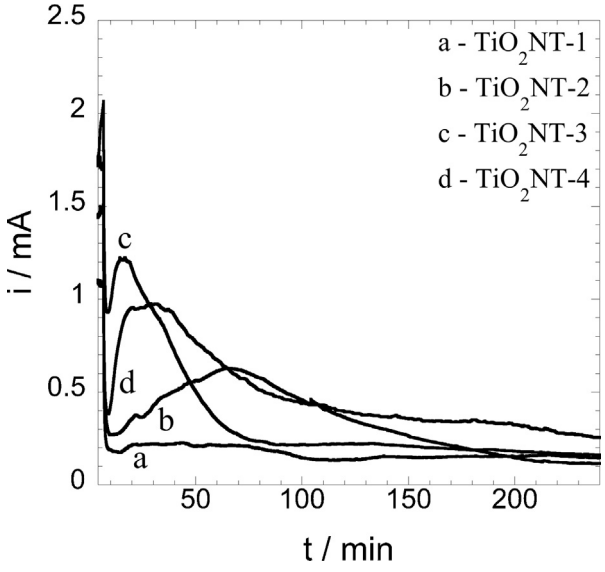

Fig. 1. Anodization current-time behaviour for Ti foil at 80 V in ethylene glycol electrolyte. *a)* TiO_2NT-1 (10 °C, 1vol.% IL), *b)* TiO_2NT-2 (10 °C, 5vol.% IL), *c)* TiO_2NT-3 (20 °C, 1vol.% IL) and *d)* TiO_2NT-4 (20 °C, 5vol.% IL). t = 240 min.

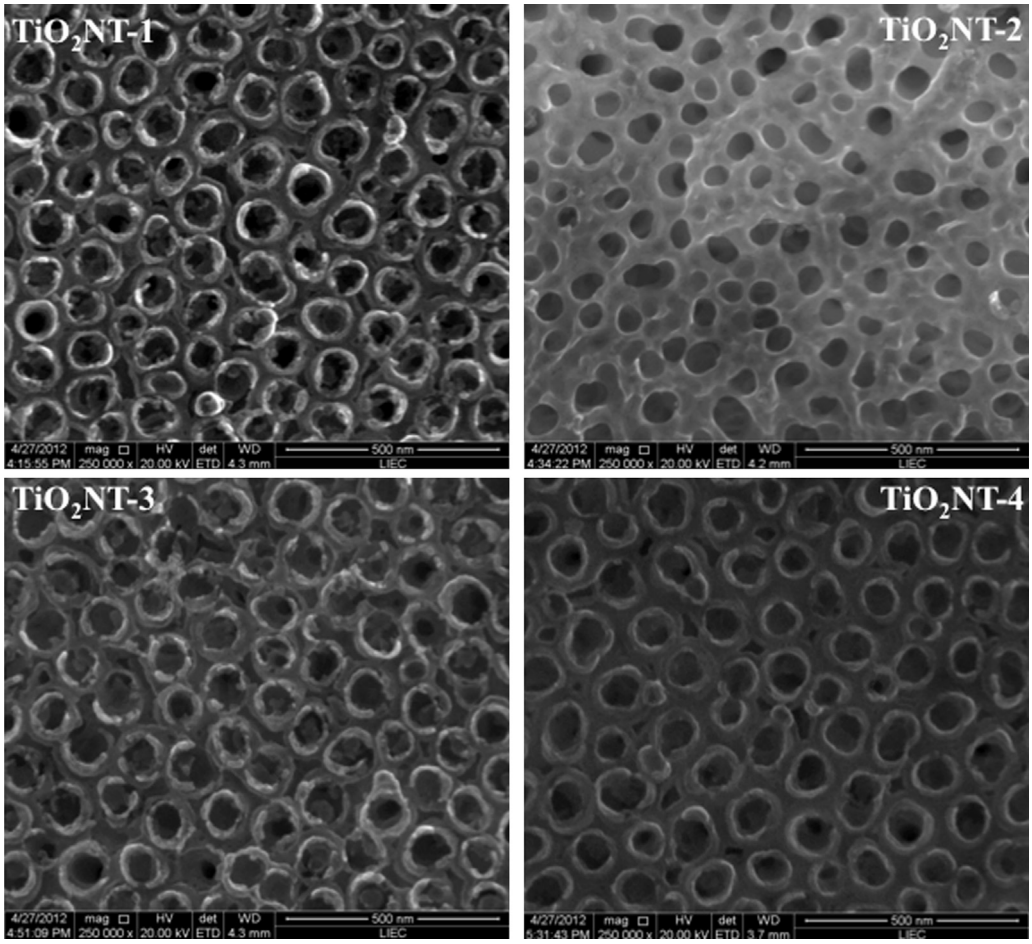

Fig. 2. FESEM images of TiO2NT arrays grown in different conditions. Tube diameter: *a)* TiO_2NT-1, *d*~77.5 ± 2.4 nm, *b)* TiO_2NT-2, *d*~64.0 ± 2.5 nm, *c)* TiO_2NT-3, *d*~75.8 ± 2.8 nm and *d)* TiO_2NT-4, *d*~68.0 ± 2.0 nm.

As can be observed by the X-ray diffraction patterns in Fig. 3, all TiO_2NT samples crystallized in the anatase phase, which is characterized by peaks at 2θ = 25.281 (101) and 2θ = 48.049 (200) (JCPDS – 21-1272). The TiO_2NT self-ordered film was thin, as metallic titanium peaks were also observed (JCPDS 44-1294) at higher intensities rather than anatase-TiO_2 ones. Also, a small amount of rutile-TiO_2 crystalline phase was detected at 2θ = 27.446 (110) and 2θ = 36.085 (101) (JCPDS – 21-1276).

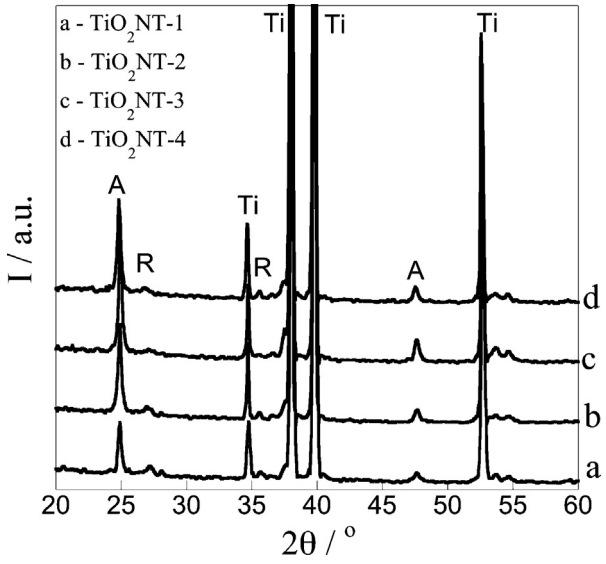

Fig. 3. XRD patterns of the TiO_2NTs arrays annealed at 450 °C for 2 hours. A, R, Ti represent anatase, rutile and titanium diffraction peaks respectively. *a)* TiO_2NT-1, *b)* TiO_2NT-2, *c)* TiO_2NT-3 and *d)* TiO_2NT-4.

The crystallite sizes (CS) were calculated using the Debye-Scherrer equation from the anatase (101) peak. The values obtained were 27.0, 28.0, 30.0 and 33.5 nm for TiO_2NT-1, 2, 3 and 4 photoelectrode respectively, as shown in Table 2. Considering the experimental error, the CS are the same for all the prepared samples. These values are similar to those previously reported in the literature [14,16] for TiO_2NT electrodes.

The band-gap, E_g, was estimated using the Tauc-Wood equation [17]:

$$(\alpha h\nu)^s = h\nu - E_g \quad (1)$$

where α is the absorption coefficient, *hν* and E_g are photon energy and optical band-gap energy, respectively. The value used for *s* was 0.5 once TiO_2 is classified an indirect gap semiconductor. E_g values were thus determined by extrapolation of the linear portion of the

Table 2
Structural and electronic parameters obtained from XRD and Mott-Schottky measurements for TiO_2NT arrays.

TiO_2NT	C.S./nm	E_{FB}/V	N_D/cm^{-3}	*w*/nm	λ_D/nm
1	27.0	1.11	6.8x1018	7.7	1.4
2	28.0	1.25	5.5x1018	6.7	1.6
3	30.0	1.2	1.5x1019	4.5	0.95
4	33.5	1.26	1.3x1019	4.2	1.0

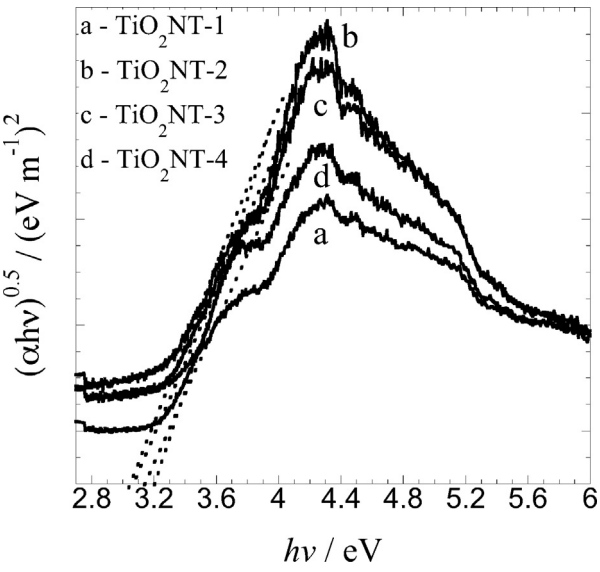

Fig. 4. Plot of $(\alpha h\nu)0.5$ vs. $h\nu$ for the estimation of the TiO_2NT band-gap energy. *a)* TiO_2NT-1, *b)* TiO_2NT-2, *c)* TiO_2NT-3 and *d)* TiO_2NT-4.

$(\alpha h\nu)^s$ curve versus the photon energy, $h\nu$, to $(\alpha h\nu)^s = 0$. Concerning the TiO_2 electronic properties of, the relevant energy levels that form the band edges, and thus, define the band-gap, are considered to be the Ti3d states and O2p levels. The lowest empty energy levels are Tid_{xy} and thus they are representative of the conduction band (CB) edge, whereas full O2p states (in particular, nonbonding $p\pi$ states) define the valence band (VB). Both anatase and rutile show this general distribution of states [18,19]. Besides, the linear dependence of $(\alpha h\nu)^{0.5}$ on $h\nu$ indicates that TiO_2 is essentially, indirect-transition-type semiconductor. The straight-line portion of the curve, when extrapolated to zero, gives the optical band-gap E_g of 3.1-3.2 eV for all TiO_2NTs-photoelectrodes, as shown in Fig. 4. The reported band-gap values of anatase phase (bulk) is 3.2 eV [20], in agreement with the anatase-TiO_2 phase observed in Fig. 3.

TiO_2 has an indirect optical band-gap for anatase (3.2 eV) and for rutile (3.0 eV). Amorphous material is reported to have a mobility gap of about 3.2–3.5 eV [18,19]. Crucial for the optical and electrical properties, is the presence of defects that provide additional states in the band-gap near the CB or VB. Particularly important to TiO_2 are oxygen vacancies and Ti^{3+} states, which, to a large extent, dominate optical and electrical properties of the material. Typically Ti^{3+} states are situated about 0.2–0.8 eV below the conduction band [21]. Electrons may be trapped in the Ti^{3+} sites or holes may be trapped in oxygen states, leading to radicals covalently bonded to the TiO_2 surface. Such shallow defects can easily release trapped charge carries to the nearby of the conduction or valence band by thermal excitation.

Systematic photoelectrochemical measurements were carried out on the TiO_2NTs photoelectrodes. Chronoamperograms were performed to examine the photoresponse over time along light on/off cycles, as shown in Fig. 5a.

The pattern of TiO_2NTs photocurrent obtained is highly reproducible for the on/off light cycles presented, Fig. 5a. Besides, the chronoamperograms profiles, Fig. 5b, are similar to those described in the literature [22–24] for water splitting on TiO_2NTs photoelectrodes. This behaviour is attributed to the photogeneration and recombination of electron-hole pairs under on/off light conditions. Under illumination, the photoinduced electrons transport from the TiO_2NT walls to the Ti substrate rapidly to produce photocurrent. Under dark conditions, the holes recombine with electrons from the TiO_2 conduction band leading to the decrease of photocurrent.

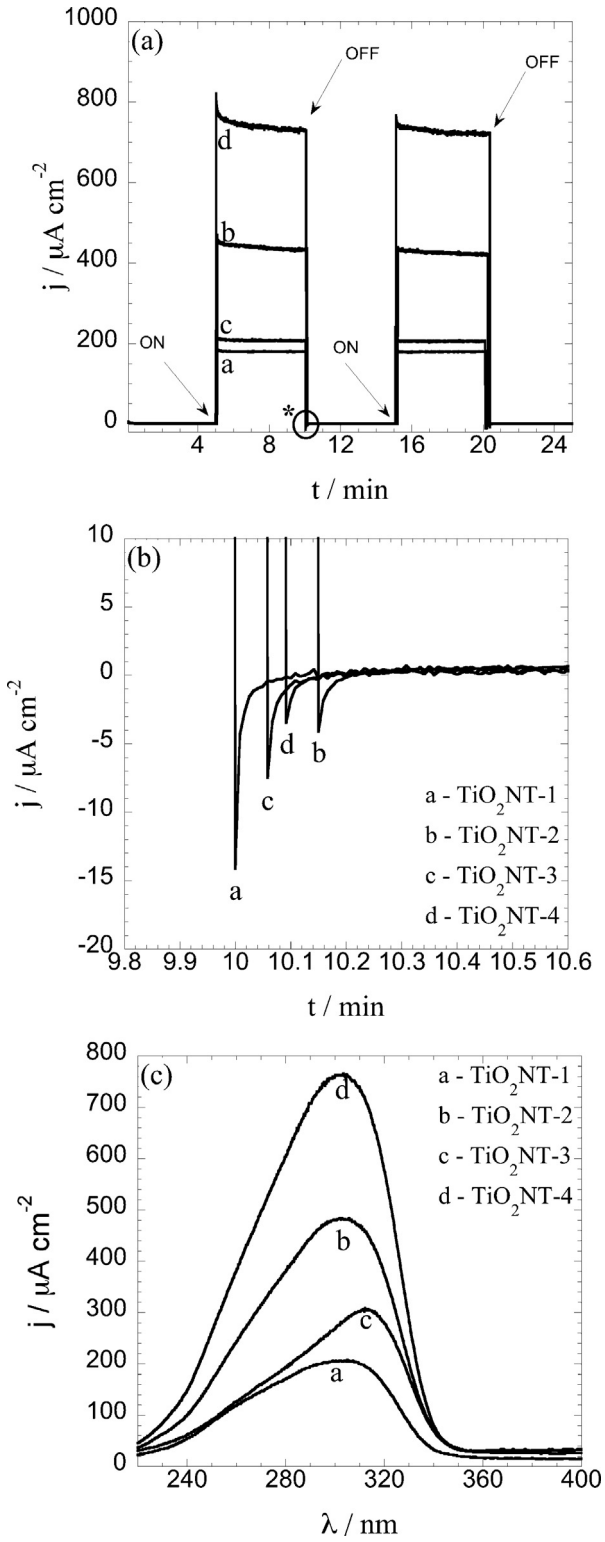

Fig. 5. *a)* Photocurrent transients generated during photoirradiation under UV-Visible light, *b)* zoomed in photocurrent transients *circled-signed in *a)* and c) photocurrent spectra. E = 0.5 V. 0.5 M H_2SO_4 electrolyte. T = 25 °C. *a)* TiO_2NT-1, *b)* TiO_2NT-2, *c)* TiO_2NT-3 and *d)* TiO_2NT-4.

The spike-like shape of photocurrent transients observed in Fig. 5b is a typical fingerprint of intense surface recombination process [25,26]. After the initial rise of photocurrent upon switching-on the light, a rapid decay is observed followed by a cathodic current "overshoot" after the light is switching-off. It

suggests that the photogenerated holes are being trapped in the surface states too deeply to induce efficient water oxidation and therefore, accumulating at the surface. This increases the probability of conduction band electrons to be captured, inducing recombination rather than photocurrents. When the light is interrupted, the holes accumulated in surface states still continue to recombine for some time, and so a cathodic current overshoot is observed. As a result, TiO_2NTs electrodes prepared at higher vol. % IL i.e. TiO_2NT-2 and 4 photoelectrodes, exhibited lower surface recombination process compared to those obtained at lower vol. % IL (TiO_2NT-1 and 3 photoelectrodes). As consequence of the lower surface recombination process exhibited by TiO_2NT-4 (observed in Fig. 5b), such photoelectrodes also exhibited higher peak photocurrent depicted by Fig. 5a and 5c, as described below.

It is possible to observe in Fig. 5a, that TiO_2NTs-2 and 4 electrodes exhibited a higher photocurrent compared to TiO_2NTs-1 and 3 photoelectrodes. One possible explanation is that higher concentration of IL leads to an increasing in the photoelectrocatalysis. Also, the photocurrent increased 305% for TiO_2NT-4, compared to the TiO_2NT-1 photoelectrode. An explanation for the increase in the peak photocurrent for higher vol. % IL TiO_2NTs prepared at the same anodization temperature, can be explained in light of Fig. 5b.

In order to estimate how the concentration of IL and the anodization temperature affect the photocurrent along the UV range, the photocurrent spectra are shown in Fig. 5c. It is possible to observe an increasing of 295% in the photocurrent for TiO_2NT-4 compared to TiO_2NT-1 photoelectrodes. This value is in agreement with that (i.e. 305%) obtained in Fig. 5a. Such increase in the photocurrent values is related to the decrease in the surface recombination process, as discussed in Fig. 5b. All TiO_2NTs show a peak wavelength around 300 nm. These peak wavelength values are in agreement with the literature. Lin et al. [27] studied the strategy of doping Fe^{3+} into TiO_2NT to enhance its photocatalytic activity. The peak photocurrent for TiO_2NT-Fe_{doped} observed was near 325 nm. Lin et al. [28] also studied the water splitting under TiO_2NT with platinum nanoparticles. The authors also observed a maximum on the incidence photon current efficiency on the UV-region. Augustynski et al. [29] observed a maximum in the photocurrent efficiency at 280 nm for nanocrystalline TiO_2 films. Finally, Jin et al. [30] studied the photoelectrooxidation of methanol in TiO_2NT, and observed a maximum in the photocurrent density near 250 nm.

Open-circuit voltage-decay (OCVD) measurements were conducted to investigate the recombination kinetics of the TiO_2NTs photoelectrodes. According to Kamat et al. [31], the open-circuit voltage of the photoelectrochemical cell represents the difference in Fermi level between TiO_2NT and counter electrodes. In the dark, the electrode potential is dictated by the redox equilibrium. Band-gap excitation of TiO_2 results in charge separation. As the holes are scavenged by H_2O at the interface, the electrons accumulate within the TiO_2NTs. Electrons accumulation causes a shift in the Fermi level to more negative potentials, and it reflects in an increase in the V_{OC}. The open-circuit voltage reaches a maximum as the electron accumulation competes with the charge recombination and this attains a steady state. Upon stopping the illumination, V_{OC} decays as the electrons accumulated within the TiO_2NT are scavenged by acceptor species in the electrolyte (e.g. H^+) as well as undergo recombination with trapped holes. Thus monitoring the decay of the voltage provides an insight into the pathways by which loss of accumulated electrons occurs within TiO_2NT.

Following the technique as reported by Bisquert et al. [32], OCVD measurements were performed by monitoring the V_{OC} transients during relaxation from an illuminated quasi-equilibrium state to the dark equilibrium, see Fig. 6-inset.

When the illumination on the TiO_2NT photoelectrodes is interrupted, the excess electrons are removed due to recombination,

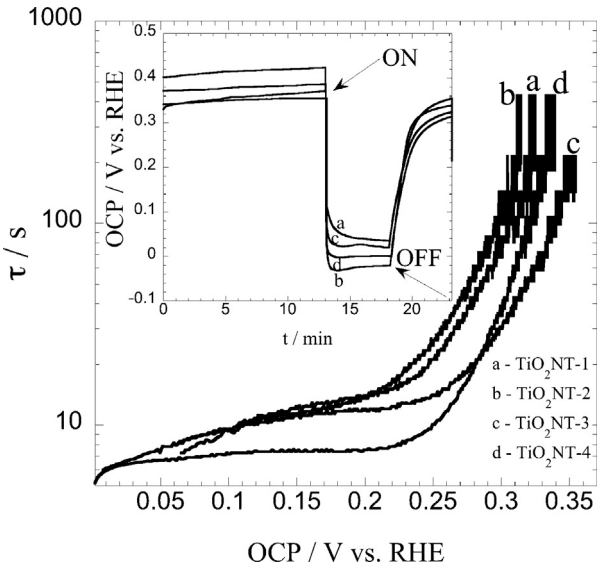

Fig. 6. Electron lifetime measurements determined form the open-circuit voltage-decay in dark-inset. Inset: the curves of open-circuit photovoltage-decay of the TiO_2NT arrays. 0.5 M H_2SO_4 electrolyte. T = 25 °C. *a)* TiO_2NT-1, *b)* TiO_2NT-2, *c)* TiO_2NT-3 and *d)* TiO_2NT-4.

with a photovoltage decay rate directly related to the electron lifetime, by the following expression:

$$\tau = \frac{k_B T}{e}\left(\frac{\partial V_{OC}}{\partial t}\right)^{-1} \quad (2)$$

where the thermal energy is given by k_BT, e is the positive elementary charge, and $\partial V_{OC}/\partial t$ is the derivative of the open circuit voltage transient. Fig. 6 is the plot of the response time obtained by applying Eq. 2 to the data in Fig. 6-inset. In general, the recombination reaction in photoelectrodes is a nonlinear property that shows a second order behaviour with respect to the electron concentration. The shape of the V_{OC} curve shows a dependence on the quasi-fermi level, confirming a trap-assisted conduction mechanism [32]. This means that the effective recombination contains contribution not only from the free carriers, but also from the trapping, detrapping and charge-transfer mechanism. Moreover, the minor delay in the electron lifetime through trapping and detrapping events is also expected considering the various TiO_2 crystallite phases encountered along the tubular structure of the TiO_2NTs. The shorter lifetimes observed at low V_{OC} in Fig. 6 are related to the charge-transfer delay.

It is possible to observe also that in comparison to reported OCVD measurements, TiO_2NT photoelectrodes prepared at higher vol.% IL (TiO_2NT-2, 4 photoelectrode) exhibited longer lifetimes prepared at the same temperature anodization. Therefore, fewer recombination centers can be observed for those samples prepared using a high vol.% IL. It is important to stress out that these data corroborates different aspects:i) the higher photocurrent observed in Fig. 5a, ii) the lower cathodic current values (spike-like shape) which could then be related to a decrease in the surface recombination process (Fig. 5b), and finally, iii) higher photocurrent values observed in Fig. 5c for TiO_2NT-4 photoelectrode.

Aiming to investigate the photoresponse of TiO_2NTs photoelectrode, i-V characteristic were also carried out by linear sweep voltammetry. In order to verify that no leakage current was present, linear sweep voltammogram of TiO_2NT-4 photoelectrode in dark conditions are also presented in Fig. 7.

The photocurrent density of TiO_2NT increases with the applied potential, and almost reaches a plateau-like behaviour at 0.7 V for all TiO_2NTs photoelectrodes. It is possible to observe that the

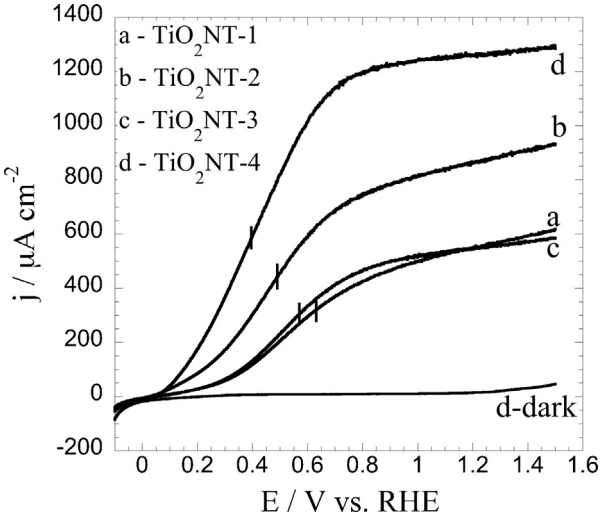

Fig. 7. Linear sweep voltammograms for TiO_2NT arrays. v = 50 mV s^{-1}. 0.5 M H_2SO_4 electrolyte. T = 25 °C. *a)* TiO_2NT-1, *b)* TiO_2NT-2, *c)* TiO_2NT-3 and *d)* TiO_2NT-4.

onset potential and the half-wave potential (short vertical line signed) shifted 250 and 260 mV respectively, towards more negative potentials for TiO_2NT-4 compared to TiO_2NT-1 samples. The negative shift of half-wave potential indicates that, the charge separation and transportation in TiO_2NT-4 photoelectrodes are more efficient. Achieve a low photocurrent onset and saturation potential is important, because it reduces the applied potential required to achieve the maximum photocurrent, and thus, increases the overall efficiency of water splitting. Moreover, it is possible to observe an increase in the peak photocurrent for TiO_2NT-4 of 130% compared to TiO_2NT-1 photoelectrodes. Finally, it is possible to observe that TiO_2NT prepared at higher vol.% IL presented higher peak photocurrent prepared at the same anodization temperature. The photoelectrocatalysis trends presented, are in agreement with those data presented in Fig. 5a, b, c and 6.

Aiming to gain information about the electronic properties of the TiO_2NT electrodes, AC impedance measurements were performed in the dark. It provides information about the intrinsic electronic properties of the semiconductor in contact with the electrolyte solution, as shown in Fig. 8.

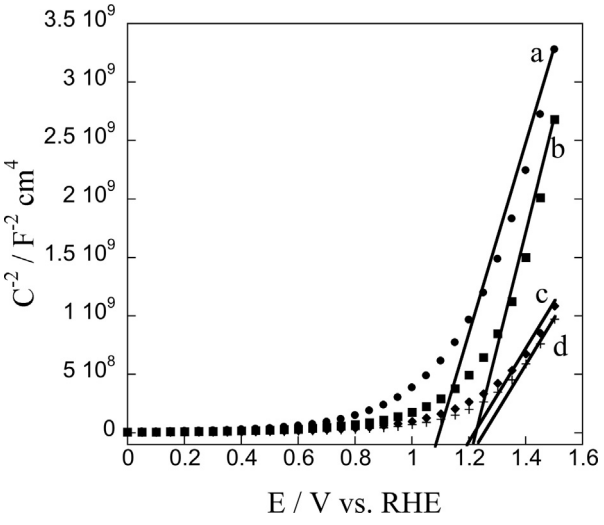

Fig. 8. Mott-Schottky plot without illumination for TiO_2NT arrays. f = 1 kHz. 0.5 M H_2SO_4 electrolyte. T = 25 °C. *a)* TiO2NT-1, *b)* TiO_2NT-2, *c)* TiO_2NT-3 and *d)* TiO_2NT-4.

Based on the Mott-Schottky plot ($1/C^2$ vs. E), one can extrapolate the position of the flatband potential E_{FB} from the x-axis intercept, which is shown in Fig. 8 and Table 2. The capacitance of the semiconductor is described by the Mott-Schottky equation:

$$\frac{1}{C^2} = \left(\frac{2}{e_0 \varepsilon \varepsilon_0 N_D}\right)\left[(E - E_{FB}) - \frac{k_B T}{e_0}\right] \quad (3)$$

wherein e_0 is the fundamental charge constant, ε the dieletric constant of TiO_2, ε_0 the permittivity of vacuum, N_D the donor density, E the electrode applied potential, E_{FB} the flatband potential, and k_BT/e_0 is a temperature-dependent correction term.

As can be seen in Fig. 8, the flatband potential calculated were 1.11, 1.25, 1.2 and 1.26 V for TiO_2NT-1, 2, 3 and 4 photoelectrodes respectively (see Table 2), and significant change in the donor density could also be observed.

The donor density (N_d) is derived by the slope of the Mott-Schottky plot and it is calculated via the equation:

$$N_D = -\left(\frac{2}{e_0 \varepsilon \varepsilon_0}\right)\left(\frac{\partial 1/C^2}{\partial V}\right)^{-1} \quad (4)$$

The donor densities were than calculated to be 6.8×10^{18}, 5.5×10^{18}, 1.5×10^{19} and 1.3×10^{19} cm^{-3} for TiO_2NT-1, 2, 3 and 4 photoelectrodes respectively. It is possible to observe that TiO_2NTs prepared at 20 °C exhibited higher donor density compared to TiO_2NTs electrodes prepared at 10 °C. Schmuki et al. [33] observed that the contribution to the photoresponse from the nanotubes is related to the annealing temperature, and, the authors used the same temperature as we did here, 450 °C. The authors observed such high doping level (10^{18}-10^{19} cm^{-3}) for TiO_2NT annealed and correlated it to the crystalline state of the material. From a different point of view, amorphous materials contain high density of recombination centers that virtually inhibit any photoconductivity in the tube walls. Zhang et al. [34] studied TiO_2 nanorods for water splitting applications. The authors obtained donor density near 4.5×10^{17} cm^{-3}. In comparison, Li et al. [35] obtained N_d values of 2×10^{18} cm^{-3} for TiO_2 nanowires prepared by a solvo-thermal route. According to the authors, such increasing in the carrier density was attributed to a high level of defects caused by oxygen vacancies. Furthermore, in the present work, one can say that the higher was the anodization temperature employed, the greater were the oxygen vacancies observed for the material, thus, the material exhibited higher carrier. As can be observed, TiO_2NT-3, 4 photoelectrodes displayed higher donor density compared to TiO_2NT-1 and 2 photoelectrodes, prepared at 20 and 10 °C respectively.

The width of the depletion layer (w), can also be derived from the Mott-Schottky plot relationship and is described by:

$$w_{dl} = \left(\frac{2\varepsilon\varepsilon_0}{e_0 N_D}\right)^{1/2}\left(E - E_{FB} - \frac{k_B T}{e_0}\right)^{1/2} \quad (5)$$

A potential of 1.5 V was chosen to calculate the width of depletion layer, and the values obtained were 7.7, 6.7, 4.5 and 4.2 nm for TiO_2NT-1, 2, 3 and 4 photoelectrodes respectively (see Table 2). Observe that, the width of depletion layer decreases for TiO_2NT obtained at higher anodization temperature. Moreover, higher vol.% IL leads to decreasing in the width of depletion layer for TiO_2NT obtained at the same anodization temperature. Munoz et al. [36] studied semiconducting properties of TiO_2NT, and also observed width of depletion layer near 7 nm. Waser et al. [37,38] studied the effect of TiO_2 thin films preparation conditions on the width of depletion layer. According to the authors [37,38] the reduction of depletion width with increasing temperature may result from a change of charge density in the depletion region. A higher temperature can help trapped charge to be released and leave behind N_D ionized sites in the depletion layer, therefore a

higher N_D leads to a thinner depletion width w, as observed and described in data presented herein.

It is important to point out, that the TiO_2NT-4 photoelectrode exhibited the lowest width of depletion layer (w = 4.2 nm). Furthermore, such photoelectrode performed the highest photoelectrocatalysis for water splitting reaction, as already discussed in Figs. 5–7. If the film thickness is of the same order of magnitude of the width of space charge region (depletion layer). Then, most of photogenerated carriers formed inside the film reach the TiO_2-electrolyte interface. Grimes et al. [39] correlated sol-gel prepared 10-540 nm TiO_2 thin films with measured photocurrent under UV illumination. A 70 nm photoelectrode showed maximum photocurrent, nearly six times higher than those of the 180-540 nm photoelectrodes. The authors suggested that films having smaller thickness than the space charge layer show a larger photocurrent due to more effective electron-hole separation. Moreover, according to Burda et al. [22] an important question for the transport of photogenerated carriers is if the depletion layer exceeds half of the tube-wall thickness. This is important because when these photogenerated electron-hole pairs form within a layer depleted of charge carriers, the likelihood is increased that they are spatially separated and add to a measurable photocurrent [40]. Therefore, changing vol.% IL and anodization temperature it is possible to modulate the width of TiO_2NT depletion layer leading to an enhancement in the photocatalysis activity. Besides, in the present case, the highest photoelectrocatalysis activity observed (TiO_2NT-4) can be related to its lowest width of depletion layer, and consequently, to a more effective electron-hole separation.

The Debey length (λ_D) gives the spatial distance needed for an effective field screening, i.e. the distance over which significant charge separation can occur. Assuming Boltzmann statistics, the Debye length decreases with increasing concentration of carriers as:

$$\lambda_D = \left(\frac{\varepsilon \varepsilon_0 k_B T}{N_D e_0^2} \right)^{1/2} \quad (6)$$

The Debye lengths obtained were 1.4, 1.6, 0.95 and 1.0 nm for TiO_2NT-1, 2, 3 and 4 photoelectrodes, respectively. It is possible to observe that higher anodization temperatures decrease Debye lengths. Trapalis et al. [41] studied anatase-TiO_2 nanoplates, and observed Debye lengths around 1.07 and 1.64 nm for samples prepared in vacuum and in air conditions respectively. Poruzet et al. [42] also studied anatase-TiO_2 nanopourous, and observed Debye lengths around 1.5 nm. These values are in agreement with those reported in this paper.

Lewis et al. [43] discussed the improvements of nanostructures compared to planar devices, and its relation towards water splitting reaction, such as decoupling of the direction of light absorption and charge-carrier collection. In order to design an efficient photoelectrode for water splitting applications, the absorber must be thick enough to absorb all the light, but also must be of sufficient electronic quality (i.e. purity and crystallinity) such that excited minority carriers that are photogenerated deep within the photoelectrodes are able to diffuse to surface, where they can be collected. As demonstrated above, TiO_2NT obtained at higher anodization temperature reduce the distance that carriers must travel, and hence enable near-unity collection efficiencies despite short minority carrier diffusion lengths. Therefore, increasing the photoelectrocatalysis activity for TiO_2NT-4 photoelectrode compared to others.

The decrease in the distance that carrier must travel leads to higher ability of carriers to diffuse to surface, where they can be collected. Such improvement on TiO_2NT prepared at higher anodization temperature, may be associated to the higher crystallite size obtained in such experimental conditions. Higher crystallite size leads to a decreasing on the density of defects (where electron-holes recombination takes place). It could also improve the diffusion coefficient, and consequently, the photoelectrocatalysis activity. Ramakrishina et al. [44] studied the improvement of electron diffusion coefficient of TiO_2 nanowires. According to the authors [44], enhanced particle size reduce the space charge region, thereby leading to an improved diffusion process. Low diffusion coefficients of TiO_2 nanoparticles can be understood by the hypothesis of electron traps in the grain boundary. Such defects could act as electron trap sites resulting from interconnection between nanoparticles. Thus, it is expected that increasing in the crystallite size could result in an improved electron transport during the water splitting reaction.

From the data described above, it is possible to conclude that was possible to prepare samples with different photoelectrochemical properties which are related to the synthesis variables conditions.

4. Conclusions

In summary, we have prepared TiO_2NT arrays photoelectrodes in ionic liquid media. Although the morphology, crystallite size and band-gap data were similar, the parameters calculated from Mott-Schottky plots revealed significant differences among the electrodes. The enhancement in the water splitting reaction obtained for the TiO_2NT-4 photoelectrode, seems to be linked to its small electron-hole recombination rate and, consequently, to a high electron lifetime.

Acknowledgements

The authors would like to thank the Brazilian Research Funding Institutions CNPq, CAPES, and FAPESP (2010/05555-2, 2012/06778-0) for financial support.

References

[1] N.S. Lewis, D.G. Nocera, Proceedings of the National Academy of Sciences 103 (2006) 15729–15735.
[2] C.A. Grimes, G.K. Mor, TiO2 Nanotube Arrays: Synthesis, Properties, and Applications, Springer, New York – USA, 2009.
[3] V.J. Babu, M.K. Kumar, A.S. Nair, T.L. Kheng, S.I. Allakhverdiev, S. Ramakrishna, International Journal of Hydrogen Energy 37 (2012) 8897–8904.
[4] Z. Zhang, M.F. Hossain, T. Takahashi, International Journal of Hydrogen Energy 35 (2010) 8528–8535.
[5] C. Richter, C.A. Schmuttenmaer, Nat Nano 5 (2010) 769–772.
[6] Y. Wu, M.K.Y. Chan, G. Ceder, Physical Review B 83 (2011) 235301.
[7] F.R. Cummings, L.J. Le Roux, M.K. Mathe, D. Knoesen, Materials Chemistry and Physics 124 (2010) 234–242.
[8] M. Salari, S.H. Aboutalebi, K. Konstantinov, H.K. Liu, Physical Chemistry Chemical Physics 13 (2011) 5038–5041.
[9] D. Wang, L. Liu, Chemistry of Materials 22 (2010) 6656–6664.
[10] V.K. Mahajan, S.K. Mohapatra, M. Misra, International Journal of Hydrogen Energy 33 (2008) 5369–5374.
[11] I. Paramasivam, J.M. Macak, T. Selvam, P. Schmuki, Electrochimica Acta 54 (2008) 643–648.
[12] S.E. John, S.K. Mohapatra, M. Misra, Langmuir 25 (2009) 8240–8247.
[13] H. Wender, A.F. Feil, L.B. Diaz, C.S. Ribeiro, G.J. Machado, P. Migowski, D.E. Weibel, J. Dupont, S.r.R. Teixeira, ACS Applied Materials & Interfaces 3 (2011) 1359–1365.
[14] J.M. Macak, H. Tsuchiya, A. Ghicov, K. Yasuda, R. Hahn, S. Bauer, P. Schmuki, Current Opinion in Solid State and Materials Science 11 (2007) 3–18.
[15] J.J. Kelly, Electrochimica Acta 24 (1979) 1273–1282.
[16] S.H. Kang, J.-Y. Kim, Y. Kim, H.S. Kim, Y.-E. Sung, The Journal of Physical Chemistry C 111 (2007) 9614–9623.
[17] D.L. Wood, J. Tauc, Physical Review B 5 (1972) 3144–3151.
[18] R. Asahi, Y. Taga, W. Mannstadt, A.J. Freeman, Physical Review B 61 (2000) 7459–7465.
[19] Z.Y. Wu, G. Ouvrard, P. Gressier, C.R. Natoli, Physical Review B 55 (1997) 10382–10391.
[20] J. Tauc, Materials Research Bulletin 5 (1970) 721–729.
[21] T.L. Thompson, J.T. Yates, Chemical Reviews 106 (2006) 4428–4453.
[22] L. Sang, H. Tan, X. Zhang, Y. Wu, C. Ma, C. Burda, The Journal of Physical Chemistry C 116 (2012) 18633–18640.
[23] H. Wu, Z. Zhang, International Journal of Hydrogen Energy 36 (2011) 13481–13487.

[24] S. Kuang, L. Yang, S. Luo, Q. Cai, Applied Surface Science 255 (2009) 7385–7388.
[25] L.M. Abrantes, L.M. Peter, Journal of Electroanalytical Chemistry and Interfacial Electrochemistry 150 (1983) 593–601.
[26] L.M. Peter, Chemical Reviews 90 (1990) 753–769.
[27] L. Sun, J. Li, C.L. Wang, S.F. Li, H.B. Chen, C.J. Lin, Solar Energy Materials and Solar Cells 93 (2009) 1875–1880.
[28] Y. Lai, J. Gong, C. Lin, International Journal of Hydrogen Energy 37 (2012) 6438–6446.
[29] R. Solarska, I. Rutkowska, J. Augustynski, Inorganica Chimica Acta 361 (2008) 792–797.
[30] Z. Zhang, Y. Yuan, Y. Fang, L. Liang, H. Ding, G. Shi, L. Jin, Journal of Electroanalytical Chemistry 610 (2007) 179–185.
[31] B.H. Meekins, P.V. Kamat, ACS Nano 3 (2009) 3437–3446.
[32] J. Bisquert, A. Zaban, M. Greenshtein, I. Mora-Seró, Journal of the American Chemical Society 126 (2004) 13550–13559.
[33] A.G. Muñoz, Q. Chen, P. Schmuki, J Solid State Electrochem 11 (2007) 1077–1084.
[34] A. Wolcott, W.A. Smith, T.R. Kuykendall, Y. Zhao, J.Z. Zhang, Small 5 (2009) 104–111.
[35] G. Wang, Q. Wang, W. Lu, J. Li, The Journal of Physical Chemistry B 110 (2006) 22029–22034.
[36] A.G. Muñoz, Electrochimica Acta 52 (2007) 4167–4176.
[37] C. Nauenheim, L. Yang, C. Kügeler, A. Rüdiger, R. Waser, RWTH Aachen (2006).
[38] L. Yang, C. Nauenheim, A. Rüdiger, H. Schroeder, R. Waser, IEEE EDS Workshop on Advanced Electron Devices (2006).
[39] C.A. Grimes, O.K. Varghese, S. Ranjan, Light, Water, Hydrogen The Solar Generation of Hydrogen by Water Photoelectrolysis, 1 ed., Springer, New York – USA, 2008.
[40] R.P. Lynch, A. Ghicov, P. Schmuki, Journal of The Electrochemical Society 157 (2010) G76–G84.
[41] K. Pomoni, M.V. Sofianou, T. Georgakopoulos, N. Boukos, C. Trapalis, Journal of Alloys and Compounds 548 (2013) 194–200.
[42] A. Hegazy, E. Prouzet, Chemistry of Materials 24 (2011) 245–254.
[43] M.G. Walter, E.L. Warren, J.R. McKone, S.W. Boettcher, Q. Mi, E.A. Santori, N.S. Lewis, Chemical Reviews 110 (2010) 6446–6473.
[44] P.S. Archana, R. Jose, C. Vijila, S. Ramakrishna, The Journal of Physical Chemistry C 113 (2009) 21538–21542.